Computational analysis of entropy generation optimization for Cu–Al_2O_3 water-based chemically reactive magnetized radiative hybrid nanofluid flow

Cite as: AIP Advances 14, 075111 (2024); doi: 10.1063/5.0213946
Submitted: 15 April 2024 • Accepted: 19 June 2024 •
Published Online: 11 July 2024

View Online Export Citation CrossMark

Govind,[1,a] Pooja Sharma,[1,b] B. K. Sharma,[2,c] Rishu Gandhi,[2,d] Bandar Almohsen,[3,e] and Laura M. Pérez[4,f]

AFFILIATIONS

[1] Department of Mathematics and Statistics, Manipal University Jaipur, Jaipur, India
[2] Department of Mathematics, Birla Institute of Technology and Science, Pilani, India
[3] Department of Mathematics, College of Science, King Saud University, Riyadh 11451, Saudi Arabia
[4] Departamento de Ingeniería Industrial y de Sistemas, Universidad de Tarapacá, Casilla 7D, Arica, Chile

[a] **Email:** govindhooda1990@gmail.com
[b] **Author to whom correspondence should be addressed:** pooja_2383@yahoo.co.in
[c] bhupen_1402@yahoo.co.in
[d] rishugandhi155@gmail.com
[e] balmohsen@ksu.edu.sa
[f] lperez@academicos.uta.cl

14 August 2024 19:06:31

ABSTRACT

This study aims to analyze the mass transfer and entropy generation in the flow system of chemically reactive, thermal radiative hybrid nanofluids (Al_2O_3/Cu with H_2O as base fluid) flow across flat stretching porous surfaces in the presence of viscous dissipation and transverse magnetic field. The governing partial differential equations are converted into a set of ordinary differential equations by applying a group of self-similarity transformations. The resulting differential equations are solved using the Bvp4c technique in MATLAB. The impact of several physical parameters has been examined the velocity, heat, and mass transfer components of the fluid. To optimize the complete heat transfer process, the consequences of all physical parameters are discussed on entropy generation and Bejan number and presented graphically. It is observed that velocity increases with the increase in magnetic parameter M because pressure force dominates over Lorentz force, temperature increases with the rise of Ec, concertation reduces with the enhancement of chemical reaction parameter delta, and the Bejan number decreases with the increase in Br; however, reverse phenomena are observed with increasing the value of the magnetic number and entropy increases with the rise of magnetic parameter M. Due to the increase in magnetic parameter M, drag force is accelerated, which leads to increase in entropy, With an increment in Pr and Ec, the heat exchange rate declines although the skin friction coefficient and mass transfer remain constant. There are several significant applications of the study of thermal analysis of hybrid nanofluid flows in numerous mechanical processes, such as extrusion or metal manufacturing processes, heat transportation in biological tissues, cooling of electric devices, high-size refrigeration, hydroelectric dams, and fuel systems.

© 2024 Author(s). All article content, except where otherwise noted, is licensed under a Creative Commons Attribution (CC BY) license (https://creativecommons.org/licenses/by/4.0/). https://doi.org/10.1063/5.0213946

I. INTRODUCTION

At the beginning of the 20th century, the theory of fluid mechanics began to grow; initially, it was based on experiments. However, there is still not much theory available, which supports the solid foundation to design the experiment. Furthermore, the theory of hydrodynamics gives significant literature that deals with flows within the region, but the concept of friction and strain has not been explained under it. Busemann and Prandtl[1] were the first scientists who could relate these two fields. In 1904, He developed the theory of boundary layers. The area where the flow changes the velocity from zero at the wall to the greatest velocity in the flow's core stream is known as a boundary layer. Blasius[2] explained the boundary layer over a flat, utilizing similarity transformation, governing differential equations that turned into third-order nonlinear ordinary differential equations, and solving it analytically in the form of power series. The literature related to this problem has been cited in the book.[3] The study of the boundary layer theory is carried out by many researchers and used in different types of fluids over different types of surfaces. Megahed *et al.*[4] studied magnetohydrodynamic laminar fluid flow due to an unsteady porous stretching sheet together with the presence of thermal radiation and variable heat flux. The impact of ohmic heating on time-dependent MHD flow past a vertical stretching sheet was examined by Sharma and Gandhi.[5] Ghoneim and Megahed[6] performed a numerical analysis of the mixed flow of a non-Newtonian Eyring–Powell fluid over a stretching sheet incorporating radiation effects. Sharma andKumawat[7] studied the influence of chemical reactions on the MHD flow of blood across a stretching surface. Tripathi and Sharma[8] investigated the impact of heat transmission on a two-phase model of blood flow. Years passed, and ordinary fluids, such as $C_2H_6O_2$, H_2O, and motor oil, were utilized for thermal transmission; however, these conventional fluids are inherently poor transmission of thermal energy. To solve this problem, solid particles were mixed into the ordinary fluid to improve heat transfer. At the beginning of the 19th century, solid particles of sized millimeters or micrometers were used to enhance heat transmission of thermal energy. However, it is observed that practical applications are not executed because of fouling, erosion, sedimentation problems, and pressure drop in the flow channel increased. Then, nano-size particles (less than 100 nm) were used to overcome this problem. A nanofluid is a fluid holding nano size (<100 nm) particle. "NANOFLUID" was first invented at the Argonne National Laboratory by Choi in 1995.[9] The study of nanofluid flows was carried out by many researchers and scientists, and because of its extensive variety of applications, it is used in the biomedical industry, power generation nuclear reactors, engine cooling, and domestic refrigerators, such as coolant. Zhang *et al.*[10] discovered that by adding a small quantity of ultrafine particles, the fluid heat transfer rate is increased approximately twice. Aluminum, copper, and carbon, nanotube particles were used as nanoparticles in a base fluid to make nanofluid fluid. Heat conduction of a nanofluid is influenced by the thermal properties of the conventional fluid and nanoparticle. Researchers[11–18] examined the nanofluid flow over different surfaces. Ghoneim and Megahed[19] investigated thermal radiative heat transfer through a thin horizontal liquid film of a Newtonian nanofluid with viscous dissipation effects subjected to a magnetic field. Previous findings show that alumina has been a pleasing nanoparticle,[20,21] because metal nanoparticles are chemically stable and immobile, but their heat conductivity is lower. Other metals, such as copper, silver, and zinc, have higher thermal conductivity. However, as stability and reactivity are constrained, metallic nanoparticles are restricted to make nanofluid. Therefore, to overcome the problem of stableness and reactivity, the amalgam of metallic nanoparticles is used in the conventional fluid. A hybrid nanofluid is a suspension of an amalgam of metal nanoparticles in conventional fluid. In a recent study, it has been observed significant improvement through hybrid nanofluid by Devi and Devi.[22] Saqib, Chamka, Sarkar *et al.*[20,23] also used alumina (Al_3O_3) in their study. Since Al_2O_3 shows lesser heat conductivity, they used an amalgam of Al_2O_3 and Cu. Stability analysis of hybrid water-based nanofluid flow with the influence of joule heating and dissipation over a shrinking surface was investigated by Rasool *et al.*[24] Mishra *et al.*[25] discussed the heat transfer of a hybrid nanofluid in the presence of viscous dissipation and Joule heating with thermal slip. Entropy generation of Cu–Al_2O_3/water flow in the presence of Joule heating and chemical reaction over a porous stretching sheet with convective boundary conditions and slip effect was discussed by Joyce *et al.*[26] Entropy analysis of Cu–Al_2O_3–H_2O hybrid nanofluid flow with melting heat transfer and nonlinear thermal radiation was investigated by Mabood *et al.*[27] The hybrid nanofluid in various dimensional plates and surfaces has been investigated by researchers, assuredly with dissimilar conditions.

The fluid is inhomogeneous because of the mixing of nanoparticles into the conventional fluid, and consequently, thermodynamics irreversibility in the flow rises, which is the main cause of heat dissipation in the system. From the thermodynamics perspective, it is essential how to create an effective heat transfer process so that the generated energy is converted into useful energy. The energy conversion process is caused by irreversibility that leads to an increase in entropy. Therefore, we need more efficient design to reduce entropy generation. In 1996, Bejan[28,29] introduced a method known as Entropy generation minimization to measure and optimize the disorder of the system during the process. There is no question that "optimize" refers to the procedure that results in the least amount of energy loss for the system. This technique, known as the second law of thermodynamics, is fulfilling its essential engineering role and thermodynamics optimization. In the 1990s, this discipline has impressively advanced. Malvandi *et al.*[30] have examined how Reynolds, Eckert, and Prandtl numbers affect entropy generation. Hedayati *et al.*[31] studied the effect of velocity ratio on the entropy on a running plate. The influence of magnetic and radiation on entropy in the MHD flow of hybrid nanofluid via tapered multi-stenosed artery was discussed by Sharma *et al.*[32] The entropy generation was analyzed by Kumawat *et al.*;[33] a two-phase blood flow for MHD using a curved permeable artery to transport heat and mass Entropy generation in nanofluid flows with various configurations has received much attention recently. The entropy of nanofluid flows for circular micro/mini channels was discussed by Sohel *et al.*[34] The impression of the Reynolds number on entropy in nanofluid flows was investigated by Moghaddami *et al.*[35] and found the optimal Reynolds number that minimizes entropy generation. By making use of the Cason fluid model, entropy generation analysis was done by Qing *et al.*[36] in MHD nanofluid flow across a porous permeable stretched plate. The entropy of $H_2O + Al_2O_3$ nanofluid is measured by Ting *et al.*[37,38]

14 August 2024 19:06:31

© Author(s) 2024

The above literature motivated the authors to work on hybrid nanofluid, especially the entropy generation of hybrid nanofluid flow. The objective of this study is to investigate the thermal and mass transfer analysis of hybrid nanofluids (Al_2O_3/Cu with H_2O as base fluid) flow across a flat porous stretching surface with thermal radiation, viscous dissipation, and chemical reaction in the presence of the transverse magnetic field. The consequence of several physical parameters, such as Eckert number, Hartmann parameter, Brinkman number, and volume fraction of nanoparticles, have been examined on entropy and Bejan number. Graphs are used to display the findings of this study, which also consider the impacts of fluid velocity, temperature, and concentration.

There are several significant applications of the study of thermal analysis of hybrid nanofluid flows in numerous mechanical processes, such as extrusion or metal manufacturing processes, heat transportation in biological tissues, cooling of electric devices, high-size refrigeration, hydroelectric dams, and fuel systems.

The novelty of this study includes:

1. Studying entropy generation provides insights into the irreversibilities and inefficiencies in the system. It helps in understanding the thermodynamic performance of the system and identifying areas where improvements can be made to enhance efficiency.
2. Suction or injection at the boundary of the flow can significantly influence the flow behavior and can be relevant in industrial processes or environmental fluid dynamics.
3. The fluid flow is taking place over a stretching porous sheet, which could represent a situation commonly encountered in industrial processes or engineering applications, such as polymer extrusion or metal forming.
4. The consideration of chemical reactions within the fluid plays a significant role, such as in reactive flows or combustion processes.

II. PROBLEM FORMULATION

A hybrid nanofluid passed through a semi-infinite plate in a uniform free stream of two-dimensional boundary layers. The hybrid nanofluid consists of two different nanoparticles Al_2O_3\Cu with H_2O as conventional fluid. Table I contains the numerical values of the thermophysical properties of Al_2O_3, H_2O, and Cu. In the recent study, the consequences of magnetic influence, infrared radiation, viscous dissipation, ohmic heating, and chemical reactions are considered, as shown in Fig. 1. The hybrid nanofluid is considered to be at rest, and there is no slip condition. In the region $X, Y \geq 0$, the fluid is flowing, the X-axis follows the stretching sheet direction and the Y-axis is the right angle to the sheet. T_w is the temperature at the plate assumed to be constant and T_∞ is the ambient temperature of the fluid. Velocity $U_w = \lambda U$ at the plate and U is the ambient velocity of the fluid, λ is the parameters for the plate velocity (Weidman *et al.*[39]) perpendicular to the stretching surface, the uniform magnetic field B_0 is applied, and S is the suction parameter. The impact of induced magnetic field is considered negligible.

TABLE I. The numerical values of the thermophysical properties of Al_2O_3, H_2O, and Cu.

Thermophysical properties	C_p (J/kg) K	ρ (kg/m^3)	k (W/Mk)	$(\sigma/\Omega\ m^{-1})$
Alumina oxide (Al_2O_3)	765	3970	40	35×10^6
Water (H_2O)	4179	997.1	0.613	5.5×10^{-6}
Copper (Cu)	385	8933	400	59.6×10^6

The governing equations for fluid flow under all the aforementioned conditions[40–42] are given as

$$\frac{\partial u}{\partial x} + \frac{\partial v}{\partial y} = 0, \tag{1}$$

$$u\frac{\partial u}{\partial x} + v\frac{\partial u}{\partial y} U\frac{\partial U}{\partial x} + \frac{\mu_{hnf}}{\rho_{hnf}}\frac{\partial^2 u}{\partial y^2} - \frac{\sigma_{hnf} B^2}{\rho_{hnf}}_{(u-U)} - \frac{\upsilon_{hnf}}{k_p^*}_{(u-U)} \tag{2}$$

$$u\frac{\partial T}{\partial x} + v\frac{\partial T}{\partial y} = \frac{k_{hnf}}{(\rho c_p)_{hnf}}\frac{\partial^2 T}{\partial y^2} - \frac{1}{(\rho c_p)_{hnf}}\frac{\partial q_r}{\partial y} + \frac{\upsilon_{hnf}}{C_P}\left(\frac{\partial u}{\partial y}\right)^2 + \frac{\sigma B^2}{(\rho c_p)_{hnf}}(u-U)^2, \tag{3}$$

$$u\frac{\partial C}{\partial x} + v\frac{\partial C}{\partial y} = D\frac{\partial^2 C}{\partial y^2} - k_r(C - C_\infty), \tag{4}$$

with boundary conditions

$$\begin{aligned} u = u_W = \lambda U,\ v = v_W\left(\frac{U v_f}{2x}\right)^{1/2} S, \\ T = T_W,\ C = C_W \quad \text{as} \quad y = 0, \\ u \to U,\ T \to T_\infty,\ C \to C_\infty \quad \text{as} \quad y \to \infty. \end{aligned} \tag{5}$$

The term $\frac{\sigma B^2}{\rho_{hnf}}$ $(u - U)$ of the right-hand side of Eq. (2) represents the Lorentz force along the x-axis and $B = \frac{B_0}{\sqrt{2x}}$ is the applied magnetic field to the fluid flow (Mahapatra *et al.*[43]). To ignore the induced magnetic field, it is considered that the magnetic Reynolds number is low. This hypothesis is justified when fluid flows, including liquid sodium and mercury, are electrically performed by Shercliff.[40] The term $\frac{\upsilon_{hnf}}{k_p^*}$ $(U\text{-}u)$ on the right-hand side of Eq. (2) represents porous permeability, $\frac{k_{hnf}}{(\rho c_p)_{hnf}}\frac{\partial^2 T}{\partial y^2}$ is the heat conduction, $\frac{\upsilon_{hnf}}{C_P}\left(\frac{\partial u}{\partial y}\right)^2$ represent the heat dissipation due to viscosity, $\frac{1}{(\rho c_p)_{hnf}}\frac{\partial q_r}{\partial y}$ represents the nanoparticles heat diffusion by radiation, and $D\frac{\partial^2 C}{\partial y^2}$ *and* $k_r(C - C_\infty)$ terms are due to the diffusion and chemical reaction, respectively.

Table II summarizes the thermophysical characteristics of hybrid nanofluid in Refs. 44 and 45. The hybrid nanofluid is a combination of 0.1 volume proportion of Cu and Al_2O_3 nanoparticles with water. In this problem, the nanoparticle Cu with 0.1 volume fraction ($\varphi_1 = 0.1$) is continuously mixed to the H_2O while the volume of fraction of Al_2O_3 (φ_2) varies to produce a hybrid nanofluid. In Table II, it is noted that the subscripts of S_1 for Cu and S_2 for Al_2O_3 nanoparticles, hnf, nf, and f, represent hybrid nanofluid, nanofluid, and fluid, respectively. However, φ_1 and φ_2 represent solid volume fractions of nanoparticles Cu and Al_2O_3.

14 August 2024 19:06:31

© Author(s) 2024

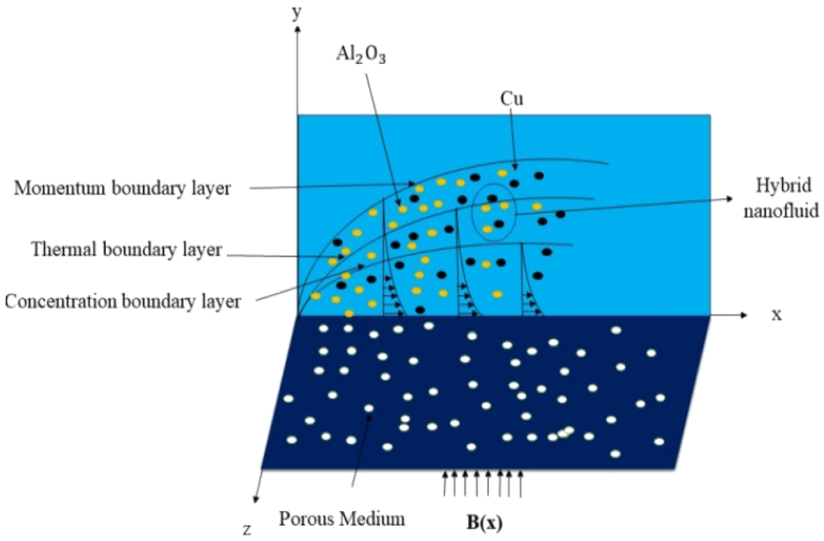


FIG. 1. Geometry of the problem.

TABLE II. Hybrid nanofluid: thermophysical characteristics.[46]

Thermophysical	Hybrid nanofluids
Density	$\rho_{hnf} = (1-\varphi_1)\left[(1-\varphi_1)\rho_f + \varphi_1\rho_{s1}\right] + \varphi_2\rho_{s2}$
Heat capacity	$(\rho C_p)_{hnf} = (1-\varphi_2)\left[(1-\varphi_1)(\rho C_p)_f + \varphi_1(\rho C_p)_{s1}\right] + \varphi_2(\rho C_p)_{s2}$
Viscosity	$\mu_{hnf} = \mu_f/(1-\varphi_1)^{2.5}(1-\varphi_2)^{2.5}$
Thermal conductivity	$k_{hnf} = \left[k_{s2} + 2k_{nf} - 2\varphi_2\left(k_{nf} - k_{s2}\right)/k_{s2} + 2k_{nf} + \varphi_2\left(k_{nf} - k_{s2}\right)\right]k_{nf}$ $k_{nf} = \left[k_{s1} + 2k_f - 2\varphi_1\left(k_f - k_{s1}\right)/k_{s1} + 2k_f + \varphi_1\left(k_f - k_{s1}\right)\right]k_f$
Electrical conductivity	$\frac{\sigma_{hnf}}{\sigma_f} = 1 + \frac{\left(\frac{\varphi_1\sigma_1+\varphi_2\sigma_2}{\sigma_f}\right)-3(\varphi_1+\varphi_2)}{2+\left(\frac{\varphi_1\sigma_1+\varphi_2\sigma_2}{(\varphi_1+\varphi_2)\sigma_f}\right)-\left(\frac{\varphi_1\sigma_1+\varphi_2\sigma_2}{\sigma_f}-(\varphi_1+\varphi_2)\right)}$

To approximate the radiative heat flux, we use the Rosseland method, according to Hossain and Takhar,[46]

$$q_r = \frac{4\sigma_1}{3k_1}\frac{\partial T^4}{\partial y}. \tag{6}$$

The Rosseland mean absorption coefficient and Stefan–Boltzmann are represented by k_1 and σ_1, respectively. Considering the temperature difference in the flow is relatively tiny, we may ignore higher order terms and expand T^4 in a Taylor series about T_∞, and if we exclude higher order terms, we get

$$T^4 \approx 4T_\infty^3 T - T_\infty^4. \tag{7}$$

Hence,

$$\frac{\partial q_r}{\partial y} = -\frac{16\sigma_1 T_\infty^3}{3k_1}\frac{\partial^2 T}{\partial y^2}. \tag{8}$$

Below is a description of the similarity transformation for converting partial differential equations into ordinary differential equations,

$$\eta = y(U/2v_f\, x)^{1/2}, \qquad \psi = (2Uv_f x)^{1/2} f(\eta),$$
$$\theta(\eta) = \frac{\mathrm{T}-\mathrm{T}_\infty}{\mathrm{T}_\mathrm{w}-\mathrm{T}_\infty}, \qquad \Phi(\eta) = \frac{\mathrm{C}-\mathrm{C}_\infty}{\mathrm{c}_\mathrm{w}-\mathrm{c}_\infty}, \qquad v_f = \frac{\mu_f}{\rho_f}. \tag{9}$$

To solve the boundary layer equation, the Stream function ψ is introduced, where

$$\mathrm{u} = -\frac{\partial\psi}{\partial y}, \qquad \mathrm{v} = \frac{\partial\psi}{\partial x}.$$

Using similarity transformation, Eqs. (2)–(4) are reduced into

$$\frac{\mu_{\frac{\mathrm{hnf}}{\mathrm{f}}}}{\rho_{\frac{\mathrm{hnf}}{\mathrm{f}}}}\mathrm{f}''' + \mathrm{ff}'' + (M + \mathrm{K_P})(1-\mathrm{f}') = 0, \tag{10}$$

14 August 2024 19:06:31

© Author(s) 2024

$$\frac{1}{P_R}\frac{\mathrm{k_{hnf}}/\mathrm{k_f}}{(\rho c_p)_{hnf}/(\rho c_p)_f}\left(1+\frac{4}{3}\mathrm{R}\right)\theta'' + f\theta'\frac{\frac{\mu_{hnf}}{\mu_f}}{\frac{\rho_{hnf}}{\rho_f}}\mathrm{E_c}(f'') + M\mathrm{E_c}\left(1-f'\right)^2 = 0, \tag{11}$$

$$\frac{1}{Le}\Phi'' + \mathrm{f}\Phi' - Re_x\delta\Phi = \mathrm{O}, \tag{12}$$

with boundary conditions,

$$\mathrm{f}'(0)=\lambda, \quad \mathrm{f}(0)=-\mathrm{S}, \quad \theta(0)=1, \quad \Phi(0)=1 \quad \text{as } \eta=0,$$

$$\mathrm{f}'\to 1, \quad \theta\to 0, \quad \Phi\to 0 \quad \text{as } \eta\to\infty. \tag{13}$$

Primes denote the derivative concerning η. The dimensionless parameters that appear in Eqs. (10)–(12) are as follows:

$\mathrm{M}=\frac{\sigma B_0^2}{\rho_{hnf}\mathrm{U}}$ is the magnetic parameter, $K_p=\frac{\upsilon_{hnf}2\mathrm{x}}{k_p^*\mathrm{U}}$ is the porous permeability parameter, $P_r=\frac{\upsilon_f}{\alpha_f}$ is the Prandtl number, $\mathrm{R}=\frac{4\sigma^*\mathrm{T}^3_\infty}{k_{hnf}\mathrm{k}^*}$ is the thermal radiation parameter, $\mathrm{E_c}=\frac{\mathrm{U}^2}{(\mathrm{T_w}-\mathrm{T}_\infty)C_p}$ is the Eckert number, $Re_x=\frac{\mathrm{xU}}{\upsilon_f}$ is the local Reynold number, $\delta=\frac{2\upsilon_f k_r}{U^2}$ is the scaled chemical reaction parameter, $Le=\frac{\upsilon_f}{D}$ is the Lewis number, and $\mathrm{Br}=P_rE_c=\frac{U^2\mu_{hnf}}{\kappa_{hnf}(T_w-T_\infty)}$ is the Brinkman number. The other important parameters are the skin friction coefficient C_f, local Nusselt number Nu_x, and the local Sherwood number Sh_x defined by

$$C_f=\frac{\hat{\tau}_w}{\rho_{hnf}U^2}, \qquad N_{ux}=\frac{x\hat{q}_w}{K_f(T_w-T_\infty)}, \qquad Sh_x=\frac{x\hat{j}_w}{D(C_w-C_\infty)}, \tag{14}$$

where $\hat{\tau}_w$, $\hat{q}_w$, and J_w are the shear stress, heat flux, and mass flux at the surface, respectively, and defined by

$$\hat{\tau}_w=\mu_{hnf}\left(\frac{\partial u}{\partial y}\right)_{y=0}, \quad \hat{q}_w=-K_{hnf}\left(1+\frac{4}{3}\mathrm{R}\right)\left(\frac{\partial T}{\partial y}\right)_{y=0},$$

$$\hat{j}_w=-D\left(\frac{\partial C}{\partial y}\right)_{y=0}. \tag{15}$$

A. Entropy generation analysis

Entropy generation measures the thermal energy of irreversibility of the process. The entropy of the system is given by the following formula:[47]

$$E_G=\frac{K_f}{T_\infty^2}\left[\frac{K_{hnf}}{K_f}+\frac{16\sigma_1 T_\infty^3}{3k_1K_f}\right]\left(\frac{\partial T}{\partial y}\right)^2+\frac{\mu_{hnf}}{T_\infty}\left(\frac{\partial u}{\partial y}\right)^2 + \frac{\mu_{hnf}}{K_pT_\infty}(\mathrm{u}-\mathrm{U})^2+\frac{\sigma B^2}{T_\infty}(\mathrm{u}-\mathrm{U})^2+\frac{D}{C_\infty}\left(\frac{\partial C}{\partial y}\right)^2. \tag{16}$$

The right-hand side first term represents entropy generation because of heat transmission; the second term represents the entropy generation as a result of viscous dissipation. The third term represents entropy generation as a result of porous permeability, and the fourth and fifth terms represent entropy generation as a result of applied magnetic field and mass transfer, respectively,

$$N_S=\frac{T_\infty^2\left(\frac{\gamma}{\eta}\right)^2}{K_{hnf}(\mathrm{T_w}-\mathrm{T}_\infty)}E_G. \tag{17}$$

Using Eq. (17) in Eq. (16), the entropy generation equation is obtained in non-dimensional form,

$$N_s=\left(\frac{K_{hnf}}{K_f}+\frac{4}{3}\mathrm{R}\right)(\theta')^2+\frac{Br}{\Omega}\{(f'')^2+\left(K_p+\frac{M}{A}\right)(1-f')^2\} + \frac{\delta\varepsilon}{\Omega^2}(\Phi')^2, \tag{18}$$

where N_s represents the entire entropy of the system. The first term of the right-hand side of the equation represents the entropy number because of the thermal effect including radiation, the second term represents the entropy number because of the magnetic field, fluid friction, and porous permeability, and the last term represents the entropy number because of the mass transfer $\varepsilon=\frac{C_w-C_\infty}{C_\infty}$ is a non-dimensional hybrid nanoparticle volume difference parameter, $\gamma=\frac{D(C_w-C_\infty)}{K_{hnf}}$ is the hybrid nanoparticle mass transfer parameter, and $\Omega=\frac{T_w-T_\infty}{T_\infty}$ is non-non–dimensional temperature parameter.

Bejan's number is described as follows:

$$Be=\frac{\text{The entropy generation as result of thermal irreversability}}{\text{The total entropy generation}}.$$

III. NUMERICAL METHODS

The system of nonlinear ordinary differential equations with a boundary condition is solved using MATLAB's bvp4c solver. The bvp4c function in MATLAB employs a collocation method to solve boundary value problems, precisely a fourth-order collocation formula. In this investigation, the default settings for bvp4c are used, which include adaptive mesh selection, a relative tolerance of 10^{-6}, and an absolute tolerance of 10^{-6}. These tolerances assure the solution's precision and stability. In addition, a sensitivity analysis has been performed to confirm the robustness of our results under different tolerance settings. The default settings have not been modified as they were sufficient for achieving convergence in the present case. For this purpose, these equations are converted into a system of first-order ordinary differential equations with BVP,

$$y^*(1)=f, \qquad y^*(1)'=f'=y(2), \qquad y^*(2)'=f''=y^*(3),$$

$$y^*(2)'=f''=y^*(3), \qquad y^*(3)'=f''',$$

$$f'''=\frac{[-y^*(1)y^*(3)-((\sigma_{hnf}/\sigma_f)M+Kp)(1-y^*(2))]}{A},$$

$$y^*(4)=\theta, \qquad y^*(4)'=\theta'=y^*(5), \qquad y^*(5)'=\theta'',$$

$$\theta''=\frac{[(\rho c_p)_{hnf}P_rK_f][-y^*(1)y^*(5)-\mathrm{AEc}(y^*(3))^2-\mathrm{MEc}\{1-y^*(2)\}^2]}{(\rho C_p)(1+4/3R)(K_{hnf})},$$

14 August 2024 19:06:31

© Author(s) 2024

$$y^*(6) = \Phi, \qquad y^*(6)' = \Phi' = y^*(7), \qquad y^*(7)' = \Phi'',$$

$$\Phi'' = Le\{(Rex\ \delta\ y^*(6)\ - y^*(1)y^*(7)\},$$

$$y(8) = N_s = \left(1 + \frac{4}{3}R\right)(y^*(5))^2 + \frac{B_r}{\Omega}((y^*3))^2 + \left(K_p + \frac{M}{A}\right)(1 - y^*(2))^2 + \frac{\gamma\varepsilon}{\Omega^2}(y^*(7))^2,$$

$$y(9) = Be = \left(1 + \frac{4}{3}R\right)(y^*(5))^2/y^*(8).$$

Boundary conditions are

$$y^*(2) = \lambda, \qquad y^*(1) = -S, \qquad y^*(4) = 1,$$

$$y^*(6) = 1 \quad \text{for } \eta = 0,$$

$$y^*(2) \to 1, \qquad y^*(4) \to 0, \qquad y^*(6) \to 0 \quad \text{as } \eta \to \infty.$$

IV. RESULTS AND DISCUSSION

For flow across a horizontal porous stretched plate, the impact of porosity, Ohmic heating, entropy, viscosity dissipation, and mass transfer have been investigated in this work. The impact of non-dimensional parameters, such as Hartman number (M), Prandtl number (Pr), radiation parameter (R), Eckert number (Ec), porosity parameter (K_p), Lewis number (Le), local Reynold number (Re_x), solid volume fraction of Cu (φ_1) and Al_2O_3 (φ_2), respectively, surface moving parameter (λ), scaled chemical parameter (δ), temperature difference parameter (Ω), (ε) non-dimensional hybrid nanoparticle volume difference parameter, hybrid nanoparticle mass transfer parameter (γ), and suction/injection parameter (S), have been discussed on temperature, velocity, and concentration profiles, Nusselt number, skin friction coefficient, Sherwood number, entropy, and Bejan number in visual and tabular presentations. For the validity of the numerical result, the comparison is done by Aladdin *et al.*[48] in the absence of a porous medium. bvp4c solver in MATLAB (Aladdin *et al.*[48]) has been used to solve numerically the set of nonlinear boundary-valued ordinary differential equations. The results are shown in the following figures. From Figs. 2(a) and 2(b), it is clear that this finding is good promise with previous research. The default values of dimensionless parameters are R = 2, Pr = 6.2, Le = 2, M = 0.1 φ_1 = 0.1, φ_2 = 0.1, Re_x = 1, δ = 0.3, Ec = 0.1, Ω = 0.5, γ = 0.5, ϵ = 0.5, λ = 0.1, and S = 1.

Figure 2(c) demonstrates that velocity increases when the magnetic parameter M is enhanced because of imposed pressure force $\frac{\sigma B^2}{\rho}U$ that overcomes Lorentz force $\frac{\sigma B^2}{\rho}u$. Figure 2(d) shows that velocity increases with the increase of Kp due to a decrease in frictional force; hence, the fluid is accelerated. Figs. 2(e) and 2(f) demonstrate that velocity increases as the volume fraction of copper increases (φ_1) and Al_2O_3 (φ_2) nanoparticles due to the high density of the Cu rate of increase in velocity lower than Al_2O_3. Figure 2(g) illustrates the velocity retards as the suction parameter value grows; however, reverse phenomena are observed with increasing value of λ in Fig. 2(h).

It is noted in Fig. 3(a) that the thickness of the thermal boundary layer decreases as the magnetic parameter rises as imposed pressure is dominant over Lorentz force. Figure 3(b) depicts that temperature increases as the Prandtl number rises near to stretching surface; however, away from the stretching surface, its behavior is reversed. Thermal diffusivity decreases with the increase in the Prandtl number, As a result, temperature decreases. Figure 3(c) illustrates that temperature boosts with the rise of Ec. Physically speaking, fluid friction of fluid particles increases with an increase in Ec; consequently, the temperature will increase.

Figures 3(d) and 3(e) show that the temperature reduces with the rise of the volume fraction of Cu (φ_1) and Al_2O_3 (φ_2) near to the stretching surface; however, away from the stretching surface, temperature increases with an increasing value of the fractional volume of nanoparticles. Furthermore, as we increase the value of the volume fraction of nanofluid, the viscosity of fluid increases, which leads increase in friction force, consequently temperature of the fluid will enhance. Figure 3(f) shows that near stretching surface temperature decreases with the rise of radiation parameter R; however, away from the stretching surface, temperature enhances due to the rise of radiation parameter R. Increase in the radiation parameter means more heat to flow, which leads to increase in the temperature of the fluid.

It may be seen in Fig. 4(a) that fluid concertation declines with the increase in Lewis number Le because for a large value of Lewis number, the molecular diffusivity and boundary layer thickness decrease. Figure 4(b) shows that the concertation declines with the increase in local Reynolds number Re_x, and Fig. 4(c) depicts that concertation reduces with the enhancement of the chemical reaction parameter delta; as we increase the chemical parameter, the solute molecules get enhance in the chemical reaction, which leads to a decline in the concentration profile.

A. Entropy and Bejan number profiles

In Figs. 5(a)–5(d), the impact of various physical parameters on Bejan number has been plotted against η. It is observed that gradually enhancing the value of the Bejan number reached its maximum value near η = 2.5 and then decreased asymptotically. Near the stretching surface, the Bejan number is very low, which shows that viscous dissipation is dominant over heat transfer. However, near η = 2.5, heat transfer dominates over viscous dissipation. Therefore, heat transfer plays an important role. Also, it is detected that the Bejan number rises with the enhancement of radiation parameter R and temperature difference parameter Ω as exposed in Figs. 5(a) and 5(b), respectively. Physically speaking, as we increase radiation parameters and temperature, the entropy will increase as a result of the Bejan number increase. Figure 5(c) illustrates that the Bejan number decreases with the increase in Br, and Fig. 5(d) explains that with the increase in the magnetic number M, the value of the Bejan number increases. Figure 5(d) depicts that the Bejan number increases with an increase in magnetic field parameter M until it attains a maximum value near η = 2.5, thereafter phenomena are reversed.

It is noted from Fig. 5(e) that entropy increases with the rise in magnetic parameter M. Due to the increase in magnetic parameter

14 August 2024 19:06:31

© Author(s) 2024

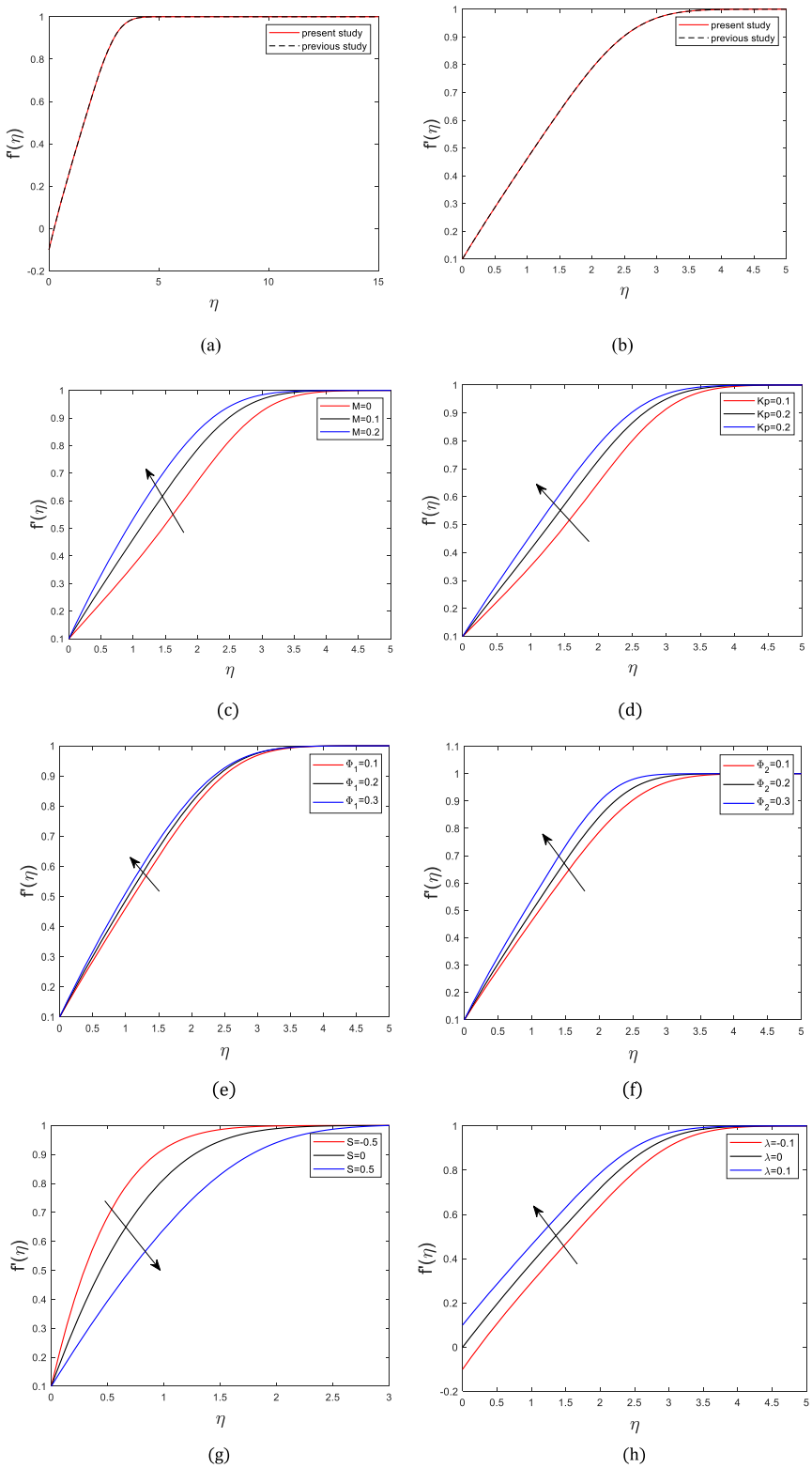


FIG. 2. (a) Comparability of velocity profile. (b) Comparability of velocity for M = 0.1 profile for λ = 0.1. (c) Impact of M on velocity. (d) Impact of Kp on velocity. (e) Impact of φ_1 on velocity. (f) Impact of φ_2 on velocity. (g) Impact of *S* on velocity. (h) Impact of λ on velocity.

14 August 2024 19:06:31

© Author(s) 2024

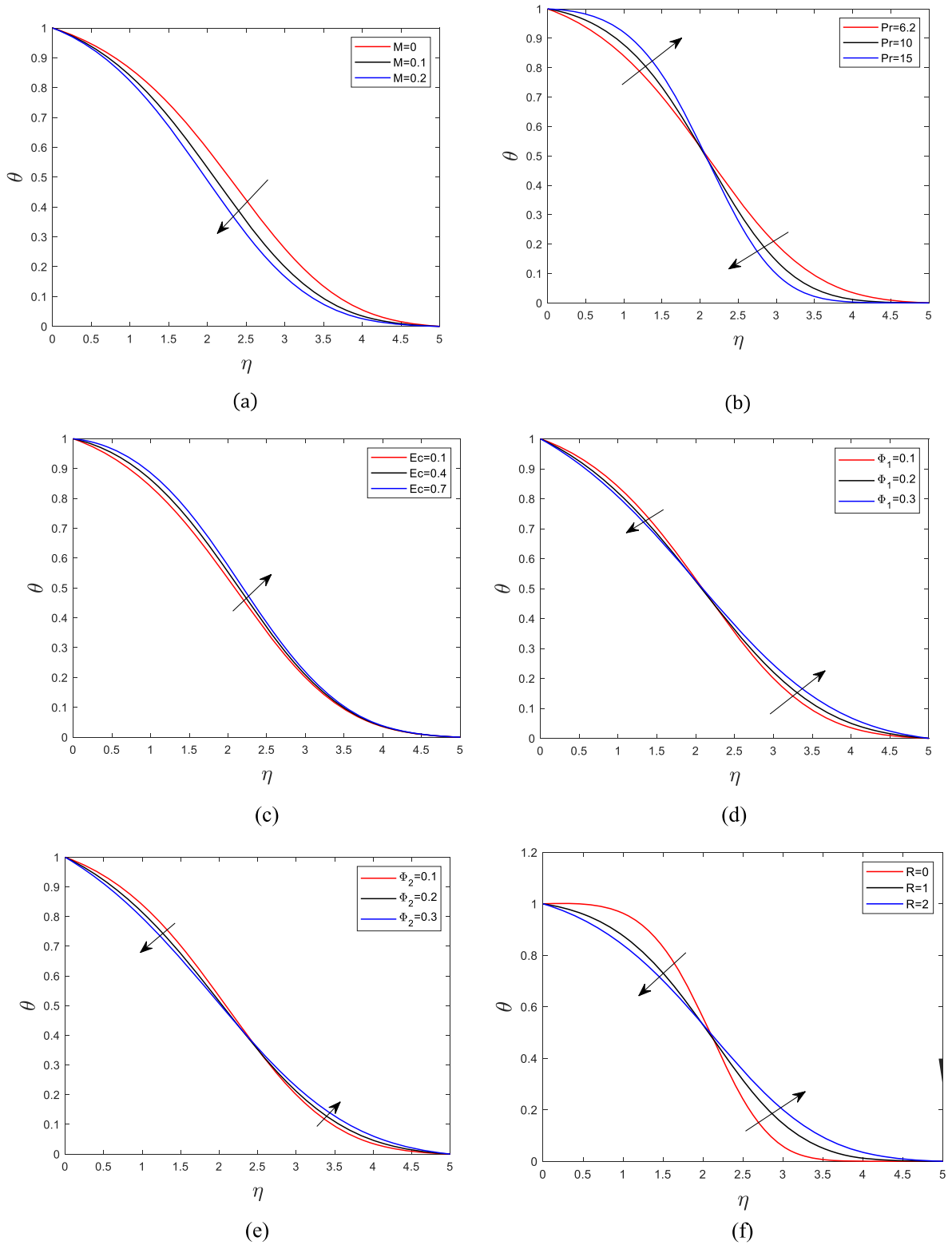


FIG. 3. (a) Impact of M on temperature. (b) Impact of Pr on temperature. (c) Impact of Ec on temperature. (d) Impact of φ_1 on temperature. (e) Impact of φ_2 on temperature. (f) Impact of R on temperature.

14 August 2024 19:06:31

© Author(s) 2024

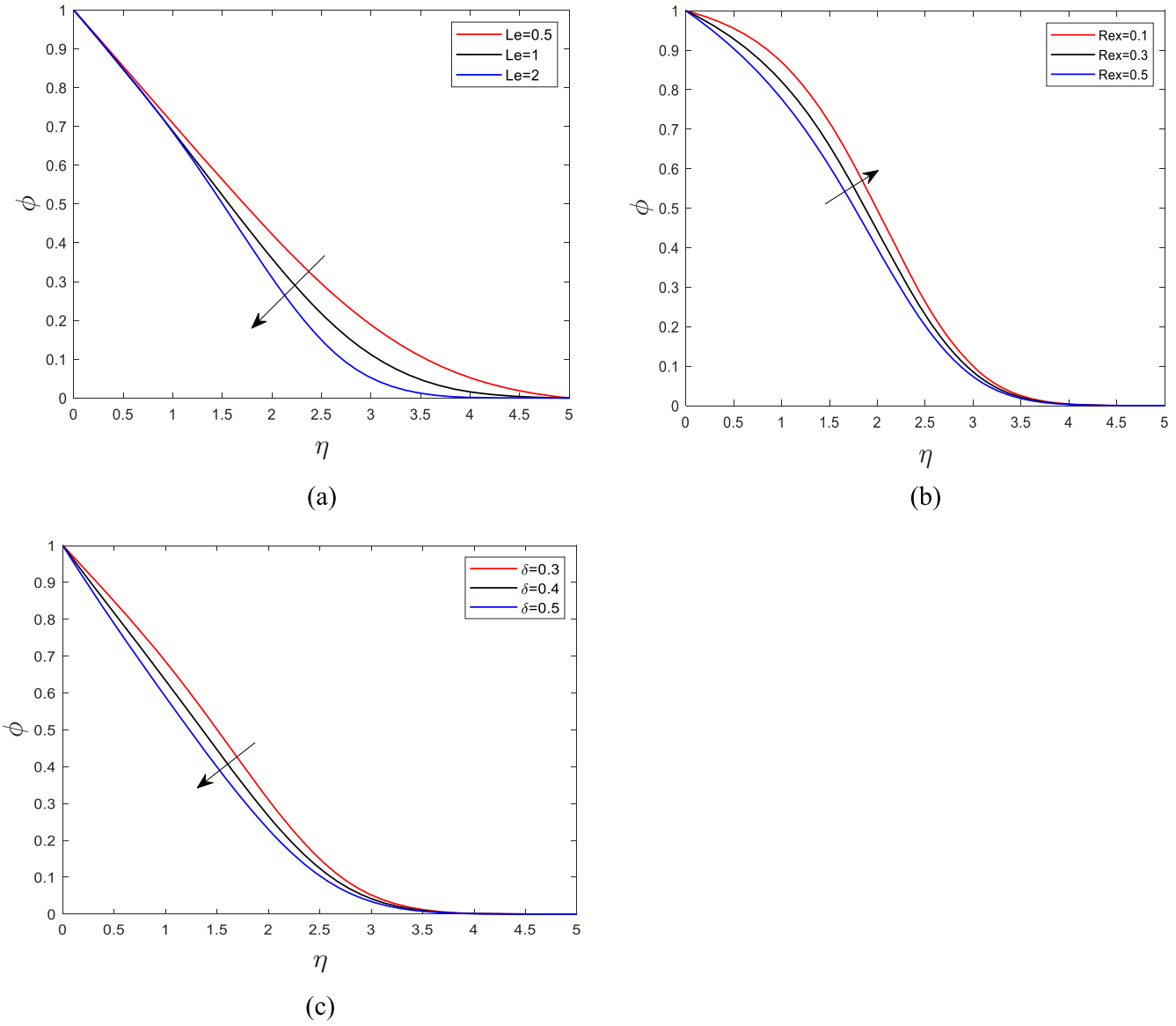


FIG. 4. (a) Impact of Le on concentration. (b) Impact of Re_x on concentration. (c) Impact of δ on concentration.

M, the drag force is accelerated, which leads to increase in entropy. Near stretching, the surface value of entropy is very high. Entropy is expanding with the increase in Brinkman number Br from Fig. 5(f). With the increase in Brinkman number Br, viscous force dominates; hence, entropy of the system is increased. Figure 5(g) illustrates that entropy increases with the enhancement of radiation parameter R, and the physical reason behind it is that when we increase the radiation parameter R in the system, we are increasing the significance of heat transfer by radiation. This increased supremacy of radiation in heat transfer naturally leads to higher levels of entropy generation due to heat transfer. Figure 5(h) depicts the impact of temperature difference parameter omega on entropy. Entropy increases with the upsurge of temperature difference parameter omega Ω.

B. Surface plots

Surface plots are three-dimensional visualizations of data. Figure 6(a) reflects that Sherwood number Sh_x decreases as the value of the Le number increases; however, in the case of φ_1, behavior is reversed. Figure 6(b) shows that the skin friction coefficient C_f increases with the increase of K_p and φ_1 due to a decrease in friction force. Figure 6(c) shows that C_f increases with the increase of M and

14 August 2024 19:06:31

© Author(s) 2024

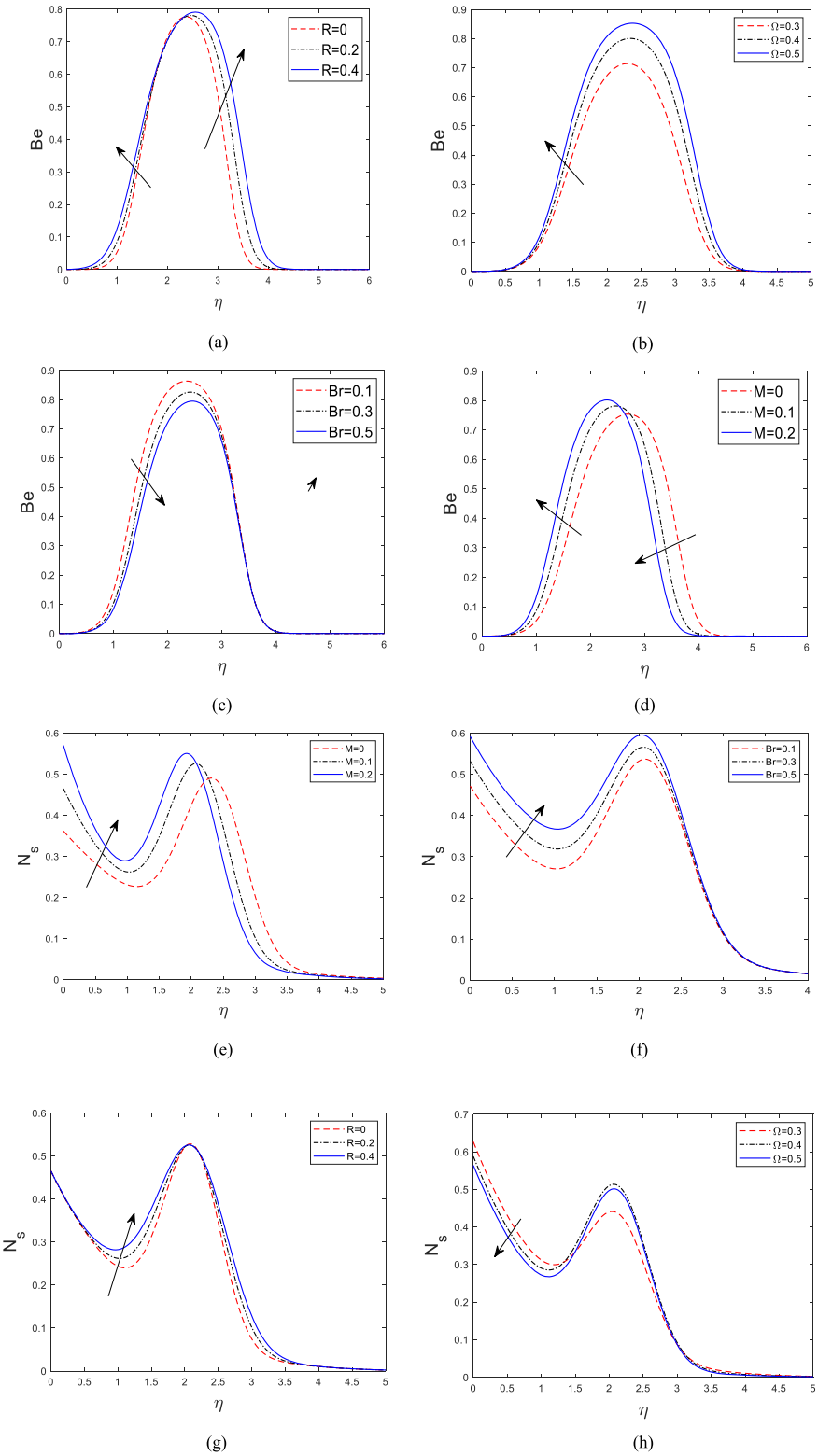


FIG. 5. (a) Impact of R on Bejan number. (b) Impact of Ω on Bejan number. (c) Impact of Br on Bejan number. (d) Impact of M on Bejan number. (e) Impact of M on entropy. (f) Impact of Br on entropy. (g) Impact of R on entropy. (h) Impact of Ω on entropy.

14 August 2024 19:06:31

© Author(s) 2024

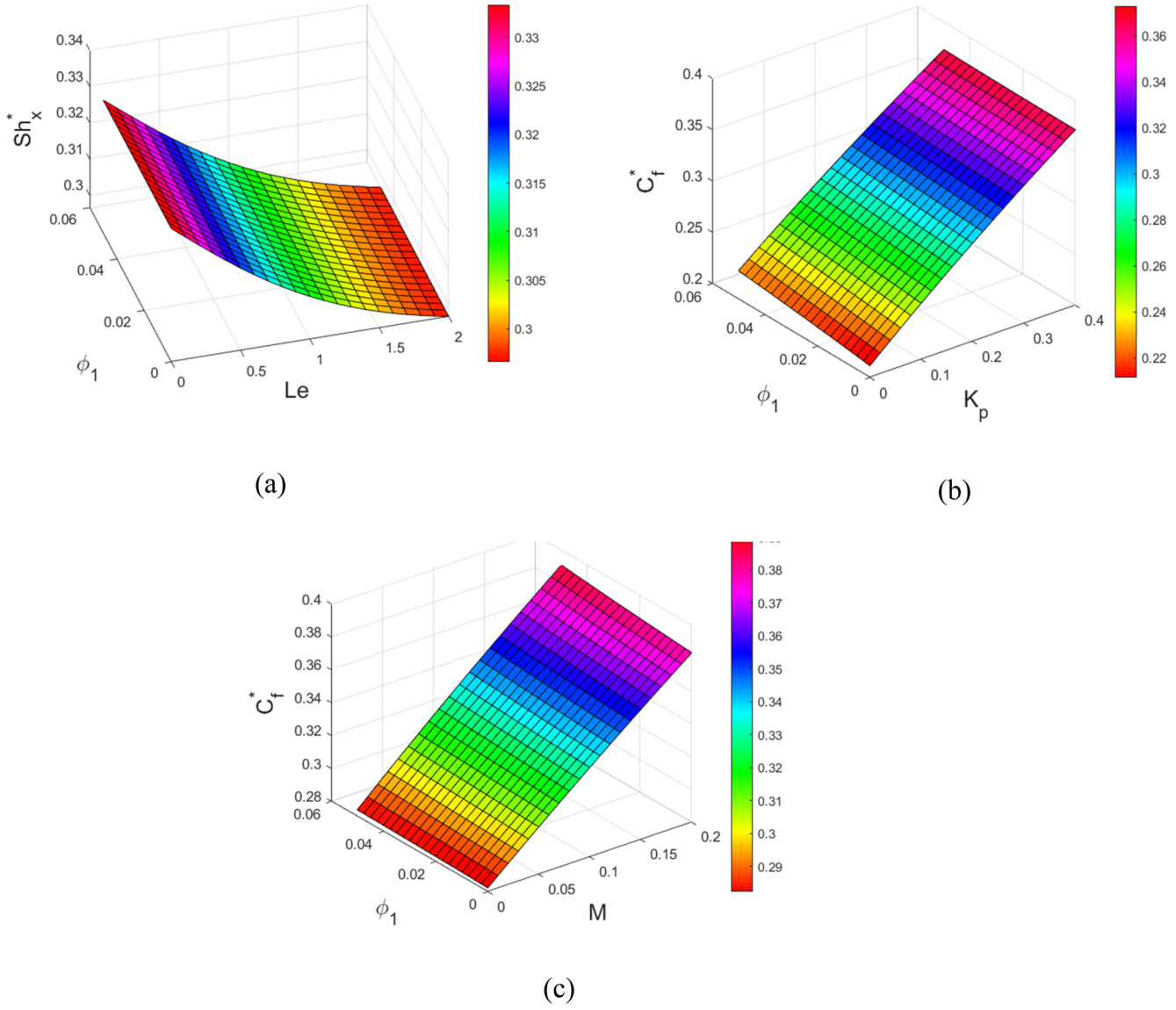


FIG. 6. (a) Impact of φ_1 and Le on Sh_x. (b) Impact of φ_1 and Kp on C_f. (c) Impact of φ_1 and M on C_f.

φ_1 since imposed pressure and M on C_f dominated over Lorentz force.

The consequence of the Prandtl number Pr, magnetic parameter M, and the Eckert number Er on the skin friction coefficient $f''(0)$, the heat exchange rate $\theta'(0)$, and the mass transport rate $\Phi'(0)$ is illustrated in Table III. The skin friction coefficient, heat exchange rate, and mass transport rate all increased with an enhancement of M. With an increment in Pr and Ec, the heat exchange rate declined although the skin friction coefficient and mass transfer remained constant.

Table IV shows how skin friction coefficient $f''(0)$, heat exchange rate $-\theta'(0)$, and mass transport rate $-\Phi'(0)$ are affected by the radiation parameter R, Lewis number Le, and porosity parameter K_P.

It has been observed that the heat exchange rate rises with an enhancement of R; however, the mass transport rate and skin friction coefficient remain constant from Table V. A decrement is observed in mass transfer with the increase of Le, while the skin friction coefficient and heat transmission remain constant. An increment is noticed in heat transfer rate, skin friction coefficient, and mass transport rate with an increment in K_p from Table V. Table VI illustrates the effect of φ_1, φ_2, Re_x, and δ on the skin friction coefficient $f''(0)$ heat exchange rate $-\theta'(0)$, and mass transport rate $-\Phi'(0)$.

14 August 2024 19:06:31

© Author(s) 2024

TABLE III. Value of various dimensionless parameters.

Parameters	Values	References
Magnetic parameter (M)	0–0.5	49
Eckert number (Ec)	0–1	50
Porous permeability parameter (K_p)	0–0.5	51
Prandtl number (Pr)	0–15	52
Radiation parameters (R)	0–5	53
Local Reynold number (Re_x)	0–0.5	
Lewis number (Le)	0–5	
Brinkman number (Br)	0–0.5	
Scaled chemical reaction parameter (δ)	0–0.8	
Temperature parameter (Ω)	0–1	
Suction/injection parameter (S)	−1–1	
Surface moving parameter	−0.5–0.5	
Solid volume fraction of Cu (φ_1)	0–0.5	
Solid volume fraction of Al_2O_3 (φ_2)	0–0.5	

TABLE IV. Comparison of $f''(0)$, $-\theta'(0)$ and, $-\Phi'(0)$ and magnetic parameter M, Prandtl number Pr, and Eckert number Ec for R = 2, Le = 2, K_p = 0.3, φ_1 = 0.1, φ_2 = 0.1, Re_x = 0.1, δ = 0.3, S = 1, and λ = 0.1.

M	Pr	Ec	$f''(0)$	$-\theta'(0)$	$-\Phi'(0)$
0.1	6.2	0.1	0.3878	0.0939	0.0651
0.2	6.2	0.1	0.500	0.1005	0.0736
0.3	6.2	0.1	0.6046	0.1050	0.0808
0.1	10	0.1	0.3878	0.0462	0.0651
0.1	15	0.1	0.3878	0.0105	0.0651
0.1	6.2	0.4	0.3878	0.0586	0.0651
0.1	6.2	0.7	0.3878	0.0233	0.0651

TABLE V. Comparison of $f''(0)$, $-\theta'(0)$ and, $-\Phi'(0)$ and radiation parameter, Lewis number Le, and porosity parameter K_p for M = 0.1, Pr = 6.2, φ_1 = 0.1, Ec = 0.1, φ_2 = 0.1, Re_x = 0.1, δ = 0.3, S = 1, and λ = 0.1.

R	Le	K_p	$f''(0)$	$-\theta'(0)$	$-\Phi'(0)$
0	2	0.3	0.3878	0.0114	0.0651
1	2	0.3	0.3878	0.0488	0.0651
2	2	0.3	0.3878	0.0939	0.0651
2	4	0.3	0.3878	0.0939	0.0347
2	6	0.3	0.3878	0.0939	0.0311
2	2	0.1	0.2449	0.0734	0.0532
2	2	0.2	0.3178	0.0848	0.0595

As the value of φ_1 and φ_2 increased, an increment in the skin friction coefficient, heat transmission rate, and mass transport rate is observed. With the increase of Re_x and δ, an increment in the mass transfer rate is noticed although the skin friction coefficient and heat transfer remained constant.

TABLE VI. Comparison of $f''(0)$, $-\theta'(0)$ and, $-\Phi'(0)$ and φ_1, φ_2, δ, and Re_x for M = 0.1, Pr = 6.2, Ec = 0.1, R = 2, K_p = 0.3, Le = 2, S = 1, and λ = 0.1.

φ_1	φ_2	Re_x	δ	$f''(0)$	$-\theta'(0)$	$-\Phi'(0)$
0.1	0.1	0.1	0.3	0.3878	0.0939	0.0651
0.2	0.1	0.1	0.3	0.4246	0.1219	0.0680
0.3	0.1	0.1	0.3	0.4650	0.1438	0.0708
0.1	0.2	0.1	0.3	0.4369	0.1263	0.0651
0.1	0.3	0.1	0.3	0.5017	0.1534	0.0749
0.1	0.1	0.2	0.3	0.3878	0.0939	0.1214
0.1	0.1	0.3	0.3	0.3878	0.0939	0.1749
0.1	0.1	0.1	0.5	0.3878	0.0939	0.0842
0.1	0.1	0.1	0.7	0.3878	0.0939	0.1030

V. CONCLUSIONS

i. Velocity increases with the increase in magnetic parameter M as imposed pressure force $\frac{\sigma B^2}{\rho} U$ overcomes Lorentz force $\frac{\sigma B^2}{\rho} u$.
ii. Velocity increases with the increase in K_p due to a decrease in frictional force.
iii. Velocity increases with the increase in volume fraction of Cu (φ_1) and Al_2O_3 (φ_2) nanoparticles as the high density of Cu rate of increase in velocity is lower than Al_2O_3.
iv. Velocity retards with the increase in the value of suction parameters S; however, reverse phenomena are observed with an increasing value of λ.
v. Thermal boundary layer thickness decreases with the increase in magnetic parameter as imposed pressure dominates over Lorentz force.
vi. Temperature increases with the increase in Ec due to an increase in fluid friction in fluid particles.
vii. Concertation decreases with the increase in Lewis number Le because for large values of Lewis number, molecular diffusivity and boundary layer thickness decrease. Concertation decreases with the increase in the local Reynolds number Re_x.
viii. Bejan number decreases with the increase in Br. The value of the Bejan number increases with the increase in magnetic parameter M parameter until it attains a maximum value near η = 2.5, thereafter phenomena are reversed.
ix. Entropy increases with the increase in magnetic parameter M and Brinkman number Br.

ACKNOWLEDGMENTS

L.M.P. acknowledges partial financial support from ANID through Convocatoria Nacional Subvención a Instalación en la Academia Convocatoria Año 2021, Grant SA77210040 and from ANID through FONDECYT 1240985. The research was supported by Researchers Supporting Project No. RSP2024R158, King Saud University, Riyadh, Saudi Arabia.

AUTHOR DECLARATIONS

Conflict of Interest

The authors have no conflicts to disclose.

14 August 2024 19:06:31

© Author(s) 2024

Author Contributions

Govind: Investigation (lead); Methodology (equal); Software (equal); Writing – original draft (equal). **Pooja Sharma**: Conceptualization (equal); Methodology (equal); Supervision (equal); Writing – review & editing (equal). **B. K. Sharma**: Conceptualization (equal); Methodology (equal); Resources (equal); Supervision (equal); Writing – review & editing (equal). **Rishu Gandhi**: Investigation (equal); Methodology (equal); Software (equal). **Bandar Almohsen**: Funding acquisition (equal); Project administration (equal); Resources (equal); Validation (equal); Writing – review & editing (equal). **Laura M. Pérez**: Formal analysis (equal); Funding acquisition (equal); Project administration (equal); Resources (equal); Validation (equal); Writing – review & editing (equal).

DATA AVAILABILITY

All data generated or analyzed during this study are included in this published article.

NOMENCLATURE

B	applied magnetic field
Be	Bejan number
Br	Brinkman number
C_f	skin friction coefficient
D_B	Brownian diffusion coefficient
Ec	Eckert number
J_w	plate mass flux
K_p	Porous permeability parameter
Le	Lewis number
M	Hartmann number
Ns	total entropy of system
Nu_x	local Nusselt number
Pr	Prandtl number
q_w	plate heat flux
R	Thermal radiation parameter
Re_x	Reynolds number
S	suction/injection parameter
Sh_x	local Sherwood number
T	temperature
U	uniform free stream
τ_w	plate shear stress

Subscripts

f	fluid
hnf	hybrid nanofluid
nf	nanofluid
w	condition on plate
∞	ambient condition

Greek Symbols

$(\rho C_P)_f$	specific heat for base fluid
C_P	specific heat at constant temperature
Ω	non-dimensional temperature parameter
λ	hybrid nanoparticle mass transfer parameter
δ	scaled chemical parameter
ϵ	non-dimensional hybrid nano particle volume difference parameter
η	similarity variable
θ	dimensional temperature
K	thermal conductivity
λ	surface moving parameter
μ	dynamic viscosity
ρ	density
σ	electrical conductivity of fluid
τ	shear stress
U	kinematic viscosity
φ	stream function

REFERENCES

[1] A. Busemann and L. Prandtl, Memoirs Fellows R. Soc. **5**, 193–205 (1960).

[2] H. Blasius, "Grenzschichten in Flussigkeiten mit Kleiner Reimbuing," Z. Math. Phys. **56**, 37 (1908).

[3] H. Schlichting and K. Gersten, *Boundary Layer Theory*, 8th ed. (Springer, Berlin, 2000).

[4] A. M. Megahed, N. I. Ghoneim, M. G. Reddy, and M. El-Khatib, "Magnetohydrodynamic fluid flow due to an unsteady stretching sheet with thermal radiation, porous medium, and variable heat flux," Adv. Astron. **2021**, 1–9.

[5] B. K. Sharma and R. Gandhi, "Combined effects of Joule heating and non-uniform heat source/sink on unsteady MHD mixed convective flow over a vertical stretching surface embedded in a Darcy-Forchheimer porous medium," Propul. Power Res. **11**(2), 276–292 (2022).

[6] N. I. Ghoneim and A. M Megahed, "Numerical analysis of the mixed flow of a non-Newtonian fluid over a stretching sheet with thermal radiation," Fluid Dyn. Mater. Process. **19**, 407–419 (2023).

[7] B. K. Sharma and C. Kumawat, "Impact of temperature dependent viscosity and thermal conductivity on MHD blood flow through a stretching surface with ohmic effect and chemical reaction," Nonlinear Eng. **10**(1), 255–271 (2021).

[8] B. Tripathi and B. K. Sharma, "Influence of heat and mass transfer on two-phase blood flow with Joule heating and variable viscosity in the presence of variable magnetic field," Int. J. Comput. Methods **17**(03), 1850139 (2020).

[9] S. U. S. Choi, "Enhancing thermal conductivity of fluids with nanoparticle," in *Developments and Applications of Non-newtonian Flows*, edited by D. A. Siginer and H. P. Wang (ASME FED, 1995), Vol. 231/MD, pp. 99–105.

[10] S. U. S. Choi, Z. G. Zhang, W. Yu, F. E. Lockwood, and E. A. Grulke, "Anomalous thermal conductivity enhancement in nanotube suspensions," Appl. Phys. Lett. **79**, 2252–2254 (2001).

[11] P. Singh and M. Kumar, "MHD slip flow of alumina water nanofluid over flat plate," in National Conf. on Synergetic Trends in Engineering And Technology (STET-2014) (IJETR), 2014, Special Issue.

[12] H. Rasheed, A. Rehman, N. Sheikh, and S. Iqbal, "MHD boundary layer flow of nanofluid over a continuously moving stretching surface," Appl. Comput. Math. **6**(6), 265–270 (2017).

[13] B. O. Falodun and S. E. Fadugba, "Effects of heat transfer o unsteady magneto-hydrodynamics (MHD) boundary layer flow of an incompressible fluid a moving vertical plate," World Sci. News. WSN **88**(2), 118–137 (2017).

[14] M. M. Junoh, F. M. Ali, N. M. Arifin, and N. Bachok, "Dual solutions in magnetohydrodynamic (MHD) flow on a nonlinear porous shrinking sheet: A stability analysis," AIP Conf. Proc. **1974**, 020083 (2018).

[15] N. H. Rahman, N. Bachok, and H. Rosali, "MHD stagnation-point flow over a stretching/shrinking sheet in nanofluids," Univ. J. Mech. Eng. **7**(4), 183–191 (2019).

14 August 2024 19:06:31

© Author(s) 2024

[16]M. Sheikholeslami, R. Ellahi, and K. Vafai, "Study of Fe_3O_4-water nanofluid with convective heat transfer in the presence of magnetic source," Alexandria Eng. J. **57**, 565–575 (2018).
[17]M. S. Ahmed, M. R. A. Hardy, and G. Abdillah, "Experimental investigation on the performance of chilled water air conditioning unit using alumina nanofluid," Therm. Sci. Eng. Prog. Chem. Org. Nat. Prod. **5**, 589–596 (2018).
[18]M. S. Ahmed and E. A. Mimi, "Effect of hybrid and single nanofluid on the performance characteristics of chilled water air conditioning system," Appl. Therm. Eng. **163**, 1359–4311 (2019).
[19]N. I Ghoneim and A. M Megahed, "Hydromagnetic nanofluid film flow over a stretching sheet with prescribed heat flux and viscous dissipation," Fluid Dyn. Mater. Process. **18**, 1373–1388 (2022).
[20]J. Sarkar, P. Ghosh, and A. Adil, "A review on hybrid nanofluids: Recent research, development and applications," Renewable Sustainable Energy Rev. **43**, 164–177 (2015).
[21]B. Takabi and H. Shokouhmand, "Effects of Al_2O_3-Cu/water hybrid nanofluid on heat transfer and flow characteristics in turbulent regime," Int. J. Mod. Phys. C **26**(04), 1550047 (2015).
[22]S. U. Devi.S and S. P. Anjali Devi, "Heat transfer enhancement of Cu-Al_2O_3/water hybrid nanofluid flow over stretching sheet," J. Niger. Math. Soc. **36**, 419–433 (2017).
[23]A. J. Chamka, I. V. Microshnichenko, and M. A. Sheremet, "Numerical analysis of unsteady conjugate natural convection of hybrid water based nanofluid in a semi-circular cavity," J. Therm. Sci. Eng. Appl. **9**(4), 041004 (2017).
[24]G. Rasool, X. Wang, U. Yashkun, L. A. Lund, and H. Shahzad, "Numerical treatment of hybrid water based nanofluid flow with effect of dissipation and Joule heating over a shrinking surface: Stability analysis," J. Magn. Magn. Mater. **571**, 170587 (2023).
[25]S. Mishra, K. Swain, and R. Dalai, "Joule heating and viscous dissipation effects on heat transfer of hybrid nanofluids with thermal slip," Iran. J. Sci. Technol. Trans. Mech. Eng. **48**, 531 (2024).
[26]M. I. Joyce, J. Kandasamy, and S. Sivanandam, "Entropy generation of Cu–Al_2O_3/water flow with convective boundary conditions through a porous stretching sheet with slip effect, joule heating and chemical reaction," Math. Comput. Appl. **28**(1), 18 (2023).
[27]F. Mabood, T. A. Yusuf, and W. A. Khan, "Cu–Al_2O_3–H_2O hybrid nanofluid flow with melting heat transfer, irreversibility analysis and nonlinear thermal radiation," J. Therm. Anal. Calorim. **143**, 973 (2021).
[28]A. Bejan, *Entropy Generation Minimization*, 2nd ed. (CRC, Boca Raton, 1996).
[29]A. Bejan, *Entropy Generation Through Heat and Fluid Flow* (Wiley, New York, 1982).
[30]M. Amir, G. D. Davood, H. Faraz, K. H. Mohhamad, and J. Moein, "Series solution of entropy generation toward an isothermal flat plate," Therm. Sci. **16**(5), 1289–1295 (2012).
[31]A. Malvandi, F. Hedayati, and D. D. Ganji, "Thermodynamic optimization of fluid flow over an isothermal moving plate," Alexandria Eng. J. **52**(3), 277–283 (2013).
[32]B. K. Sharma, R. Gandhi, and M. M. Bhatti, "Entropy analysis of thermally radiating MHD slip flow of hybrid nanoparticles (Au-Al_2O_3/Blood) through a tapered multi-stenosed artery," Chem. Phys. Lett. **790**, 139348 (2022).
[33]C. Kumawat, B. K. Sharma, Q. M. Al-Mdallal, and M. Rahimi-Gorji, "Entropy generation for MHD two phase blood flow through a curved permeable artery having variable viscosity with heat and mass transfer," Int. Commun. Heat Mass Transfer **133**, 105954 (2022).
[34]M. R. Sohel, R. Saidur, N. H. Hassan, M. M. Elias, S. S. Khaleduzzaman, and I. M. Mahbubul, "Analysis of entropy generation using nanofluid flow through the circular microchannel and minichannel heat sink," Int. Commun. Heat Mass Transfer **46**(0), 85–91 (2013).
[35]M. Moghaddami, S. Shahidi, and M. Siavashi, "Entropy generation analysis of nanofluid flow in turbulent and laminar regimes," J. Comput. Theor. Nanosci. **9**(10), 1586–1595 (2012).
[36]J. Qing, M. M. Bhatti, M. A. Abbas, M. M. Rashidi, and M. E.-S. Ali, "Entropy generation on MHD Casson nanofluid flow over a porous stretching/shrinking surface," Entropy **18**(4), 123 (2016).
[37]T. W. Ting, Y. M. Hung, and N. Guo, "Entropy generation of viscous dissipative nanofluid convection in asymmetrically heated porous microchannels with solid-phase heat generation," Energy Convers. Manage. **105**, 731–745 (2015).
[38]T. W. Ting, Y. M. Hung, and N. Guo, "Entropy generation of viscous dissipative nanofluid flow in thermal non-equilibrium porous media embedded in microchannels," Int. J. Heat Mass Transfer **81**, 862–877 (2015).
[39]P. D. Weidman, D. G. Kubitschek, and A. Davis, "The effect of transpiration on self-similar boundary layer flow over moving surfaces," Int. J. Eng. Sci. **44**, 730–737 (2006).
[40]E. Haile and B. Shankar, "Boundary layer flow of nanofluids over a moving surface in the presence of thermal radiation, viscous dissipation and chemical reaction," Appl. Appl. Math. Int. J. **10**(2), 952–969 (2015).
[41]N. Bachok, A. Ishak, and I. Pop, "Boundary-layer flow of nanofluids over a moving surface in a flowing fluid," Int. J. Therm. Sci. **49**, 1663–1668 (2010).
[42]A. T. Olatundun and O. D. Makinde, *Analysis of Blasius Flow of Hybrid Nanofluids over a Convectively Heated Surface* (Trans Tech Publication, Switzerland, 2017), pp. 29–34.
[43]T. R. Mahapatra, S. K. Nandy, and A. S. Gupta, "Momentum and heat transfer in MHD stagnation-point flow over a shrinking sheet," J. Appl. Mech. **78**, 1–8 (2011).
[44]J. A. Shercliff, *A Textbook of Magnetohydrodynamics* (Pergamon, Oxford, 1965).
[45]H. F. Oztop and E. Abu Nada, "Numerical study of natural convection in partially heated rectangular enclosures filled with nanofluids," Int. J. Heat Fluid Flow **29**, 1326–1336 (2008).
[46]S. P. A. Devi and S. S. U. Devi, "Numerical investigation of hydromagnetic hybrid Cu–Al_2O_3/water nanofluid flow over a permeable stretching sheet with suction," Int. J. Nonlinear Sci. Numer. Simul. **17**(5), 249–257 (2016).
[47]M. A. Hossain and H. S. Takhar, "Radiation effect on mixed convection along a vertical plate with uniform surface temperature," Heat Mass Transfer **31**, 243 (1996).
[48]N. A. L. Aladdin, I. Pop, and N. Bachok, "Cu-Al_2O_3/water hybrid nanofluid flow over a permeable moving surface in presence of hydromagnetic and suction effects," Alexandria Eng. J. **59**, 657–666 (2020).
[49]R. Gandhi, B. K. Sharma, Q. M. Al-Mdallal, and H. V. R. Mittal, "Entropy generation and shape effects analysis of hybrid nanoparticles (Cu-Al_2O_3/blood) mediated blood flow through a time-variant multi-stenotic artery," Int. J. Thermofluids **18**, 100336 (2023).
[50]R. Gandhi, B. K. Sharma, and O. D. Makinde, "Entropy analysis for MHD blood flow of hybrid nanoparticles (Au–Al_2O_3/blood) of different shapes through an irregular stenosed permeable walled artery under periodic body acceleration: Hemodynamical applications," J. Appl. Math. Mech. e202100532 (published online) (2022).
[51]B. K. Sharma, R. Gandhi, N. K. Mishra, and Q. M. Al-Mdallal, "Entropy generation minimization of higher-order endothermic/exothermic chemical reaction with activation energy on MHD mixed convective flow over a stretching surface," Sci. Rep. **12**(1), 17688 (2022).
[52]R. Gandhi, B. K. Sharma, C. Kumawat, and O. A. Beg, "Modeling and analysis of magnetic hybrid nanoparticle (Au-Al_2O_3/blood) based drug delivery through a bell-shaped occluded artery with joule heating, viscous dissipation and variable viscosity effects," Proc. Inst. Mech. Eng., Part E **236**(5), 2024–2043 (2022).
[53]B. K. Sharma, A. Kumar, R. Gandhi, M. M. Bhatti, and N. K. Mishra, "Entropy generation and thermal radiation analysis of EMHD Jeffrey nanofluid flow: Applications in solar energy," Nanomaterials **13**(3), 544 (2023).

14 August 2024 19:06:31

© Author(s) 2024